Wideband Precoding for RIS-Aided THz Communications

Ruochen Su, *Graduate Student Member, IEEE*, Linglong Dai, *Fellow, IEEE*, and Derrick Wing Kwan Ng, *Fellow, IEEE*

***Abstract*— Reconfigurable intelligent surface (RIS)-aided terahertz (THz) communication has been considered as a promising technology for enabling future sixth-generation (6G) wireless systems. Due to the exploitation of extremely large bandwidth and large scale of RIS, RIS-aided THz communications would suffer from the beam split effect, where the generated beams cannot be aligned with the target physical direction in the whole bandwidth, so a severe array gain loss will be introduced. In this paper, the beam split effect is first analyzed in the existence of RIS. Then, a novel sub-connected RIS architecture is proposed to mitigate the beam split effect. The crux is to introduce additional time-delay (TD) modules and phase shifters into RIS elements so as to convert the classical phase-only precoding to the joint phase and delay precoding. Accordingly, a wideband precoding design is proposed to compensate for the severe array gain loss, and the performance analysis on the array gain is also provided. After that, we extend our discussions to the emerging scenarios with massive antennas equipped at the base station (BS), where the effect of "double beam split", i.e., the coupling of beam split at the BS and the RIS, occurs. We prove the decomposability of the array gain, based on which the double beam split effect can be addressed by separately optimizing the wideband precoding at the BS and the RIS. Simulation results demonstrate that our proposed sub-connected RIS significantly alleviates the beam split effect with a small number of TD modules, and it is capable of achieving sub-optimal achievable rate performance with acceptable hardware cost and power consumption.**

***Index Terms*— Reconfigurable intelligent surface (RIS), terahertz (THz) communications, double beam split, wideband precoding.**

I. Introduction

THE peak data rate is one of the key performance indicators (KPIs) for future sixth-generation (6G) wireless communications [1]. One of the most effective approaches to realizing a high data rate is to adopt a large system bandwidth. Compared with the existing fifth-generation (5G) communications operating at sub-6 GHz with a typical bandwidth of 100 MHz, terahertz (THz) communications at the frequency band of 0.1-10 THz enjoy tens of GHz unlicensed bandwidth [2]. Thanks to the rich spectral resources, THz communication is able to support a peak data rate of up to Tbps for emerging applications, e.g., augmented reality, holographic telepresence, etc. As such, it has been perceived as a disruptive technology to enable future 6G wireless networks [3]. However, since the inherent blockage-susceptible characteristic of THz signals leads to a high dependence on line-of-sight (LoS) paths [4], the data rate performance of THz communication is generally poor when there are no LoS paths. Fortunately, the reconfigurable intelligent surface (RIS) is capable of providing extra signal propagation paths that effectively addresses the blockage problem by proactively manipulating the wireless environment [5], [6]. Thus, RIS-aided THz communication is appealing for the realization of future 6G wireless systems [7]. Similar to THz massive multiple-input multiple-output (MIMO) [8], a large number of antennas at the base station (BS) and a large number of elements at the RIS are usually exploited to generate highly directional and energy-focused beams to compensate the severe signal propagation attenuation in THz communications.

A. Prior Works

Recently, RIS has attracted extensive research interests from both industry and academia. The primary studies include precoding design [9], [10], [11], [12], channel acquisition [13], [14], [15], [16], architecture design [17], [18], etc. Existing works of RIS are mainly considered in the narrowband scenarios. For example, the received signal power at the user was analytically maximized in multiple RISs-aided communication systems [9]. Moreover, the precoding at the BS and the phase shifting at the RIS were alternately optimized by the block coordinate descent method to maximize the weighted sum-rate of all the considered users [11]. More recently, several works have discussed RIS-aided wideband systems, especially in THz bands [19], [20], [21], [22], [23], [24]. For instance, a swarm intelligence-based beamforming method was proposed for RIS-aided THz communications, based on which the ergodic capacity was derived [21]. The authors developed a beam training and alignment method by solving a joint sparse sensing and phaseless estimation problem based

Manuscript received 2 November 2022; revised 5 February 2023 and 11 March 2023; accepted 13 March 2023. Date of publication 29 March 2023; date of current version 16 June 2023. This work was supported by the National Key Research and Development Program of China (Grant No. 2020YFB1807201) and in part by the National Natural Science Foundation of China (Grant No. 62031019). This work was also supported by the Australian Research Council's Discovery Project (DP210102169, DP230100603). The associate editor coordinating the review of this article and approving it for publication was H. Tabassum. *(Corresponding author: Linglong Dai.)*

Ruochen Su and Linglong Dai are with the Department of Electronic Engineering, Tsinghua University, Beijing 100084, China, and also with the Beijing National Research Center for Information Science and Technology (BNRist), Beijing 100084, China (e-mail: src18@mails.tsinghua.edu.cn; daill@tsinghua.edu.cn).

Derrick Wing Kwan Ng is with the School of Electrical Engineering and Telecommunications, the University of New South Wales, Sydney, NSW 2052, Australia (e-mail: w.k.ng@unsw.edu.au).

Color versions of one or more figures in this article are available at https://doi.org/10.1109/TCOMM.2023.3263230.

Digital Object Identifier 10.1109/TCOMM.2023.3263230

on the sparse structure of RIS-related cascade channels [22]. Besides, a deep reinforcement learning-based beamforming design was investigated to improve the coverage range in multi-hop RIS-aided THz communications [23].

Despite various efforts have been devoted, most existing RIS precoding schemes, e.g., [9], [10], [11], [12], [19], [20], [21], [22], [23], and [24], do not work well when the signal bandwidth is enormous (e.g., several GHz), especially in practical THz communication systems. Specifically, since a practical RIS is usually equipped with *frequency-independent* phase-shifting circuits [9], [10], RIS-aided communications can only perform frequency-independent precoding. For RIS-aided THz communications with massive RIS elements, the generated beams at different subcarrier frequencies by the mentioned conventional methods would point to different physical directions. This phenomenon is known as "beam split", which is more serious than beam squint in millimeter-wave communications [8], [25], [26], [27], [28], [29], [30], [31]. In comparison, the generated beams slightly squint at different subcarriers due to beam squint, which are still able to cover the target [8], [26], [27]. Since the scale of a RIS is usually larger than that of a BS [32], [33], the performance loss caused by the beam split effect in the existence of RIS becomes more serious. For example, for a typical scenario with 100 GHz center frequency, 10 GHz bandwidth, 128 subcarriers, and 64×64 RIS elements, it can be shown that the array gain loss is up to 80% at almost half of all available subcarriers.

In the literature, only a few recent works have considered the effect of beam split in RIS-aided wideband communications, which are generally classified into two categories. The first category of solutions deals with beam split by the application of advanced optimization algorithms [27], [28]. In particular, the authors in [27] maximized the upper bound of the achievable rate to mitigate beam split by utilizing the channel covariance matrix and long-term angle information. Besides, the relationship between the deployment of RIS and the beam split effect was studied in [28]. Although the distributed RIS deployment with high cost can alleviate the beam split effect, the corresponding received signals would suffer from significant energy loss due to the shrinkage of the surface aperture. It is worth noting that all of these methods [27], [28] still rely on the frequency-independent precoding architecture. As a result, the beam split effect can only be slightly alleviated to a certain extent. Indeed, when the bandwidth is sufficiently large, e.g., in THz communication systems, the negative impacts of beam split would be magnified, and these approaches still suffer from a severe loss in beamforming gain. The second category of solutions relies on hardware improvement. For example, the varactor diodes-based delay adjustable metasurface was introduced in [29], which can control the electromagnetically induced transparency properties and thus impose extra time delay. Owing to the *frequency-dependent* precoding achieved by the introduced delay based on such time-delay (TD) modules, this approach can completely overcome beam split from the theoretical perspective. However, the required number of TD modules has to be equal to the number of massive RIS elements, leading to excessive hardware cost and power consumption. In fact, the second category of solutions is less attractive than the first one for practical implementation.

In summary, to the best of our knowledge, there are no practical wideband precoding solutions for RIS-aided THz communications to effectively address beam split, where the balance between the beamforming gain and the hardware cost as well as power consumption should be considered.

B. Contributions

In this paper, we propose a wideband precoding technique to address the beam split effect with an affordable hardware cost.[1] The main contributions are summarized as follows.

- To alleviate the performance degradation resulting from the beam split effect of RIS at an acceptable hardware cost, we propose a new sub-connected architecture-based RIS with a small number of TD modules. Specifically, each element of the sub-array of RIS is equipped with two-layer phase shifters and is connected to a common TD module. The received signal at each element passes through the first-layer phase shifter, the common TD module, and the second-layer phase shifter in turn. The proposed sub-connected architecture can convert the classical phase-only narrowband precoding to the joint phase and delay wideband precoding, which achieves a better tradeoff between the data rate and the hardware cost as well as the power consumption.
- We propose a frequency-dependent wideband precoding design based on the proposed sub-connected architecture. Specifically, the first-layer phase shifters at the sub-array aim at creating constructive interference superimposed signals received by different elements. The second-layer phase shifters at the sub-array generate a beam towards the user equipment at the center frequency. More importantly, the common TD module facilitates the alignment between the generated beams over all the subcarriers and the target physical direction. We also analyze the normalized array gain and the mechanism of the proposed wideband precoding scheme, which unveils that it effectively compensates for the severe gain loss due to beam split. It is shown that 95% array gain can be obtained in the whole bandwidth. In addition, the practical implementation with low-resolution phase shifters is also discussed to further reduce the hardware cost and power consumption.
- Furthermore, we extend our discussions from the single antenna to massive antennas at the BS, where a "double beam split" effect at the BS and RIS will be introduced. Specifically, the generated beams of the BS at different subcarriers point to different physical directions. The impinging beams and the reflected beams of the RIS also split into separated physical directions. We carry out the analysis of the array gain and prove its decomposability under LoS-dominant conditions by considering the double beam split effect. In specific, the array gain can be decomposed to the product of the normalized array gain

[1] Simulation codes are provided to reproduce the results in this paper: http://oa.ee.tsinghua.edu.cn/dailinglong/publications/publications.html.

of RIS and that of the BS. Based on the decomposability, the wideband precoding design at the RIS and the BS can be decoupled without loss of optimality, so they can be separately optimized by our proposed wideband precoding technique. Simulation results demonstrate that the proposed sub-connected architecture-based wideband precoding design effectively achieves sub-optimal achievable rate performance with strong robustness in a wide bandwidth range.

C. Organization and Notations

Organization: The rest of this paper is organized as follows. We introduce the system model of the RIS-aided THz communication in Section II. The beam split effect and the resultant array gain loss are analyzed in Section III. A sub-connected architecture and the corresponding wideband precoding design are proposed in Section IV followed by the analysis of the double beam split effect. Simulation results are provided in Section V, followed by the conclusions in Section VI.

Notations: Lower-case and upper-case boldface letters denote vectors and matrices, respectively. $\mathrm{diag}(\mathbf{a})$ represents a diagonal matrix with diagonal elements chosen from the entries of vector $\mathbf{a}$. The transpose, the conjugate transpose, and the (i,j)-th entry of matrix $\mathbf{A}$ are represented by $\mathbf{A}^T$, $\mathbf{A}^H$, and $\mathbf{A}(i,j)$, respectively. $|\mathbf{a}|$ denotes the Euclidean norm of vector $\mathbf{a}$. $E[X]$ represents the expectation of random variable X. $\mathcal{U}(a,b)$ denotes the uniform distribution between a and b. $\mathrm{sum}(\mathbf{A})$ denotes the sum of elements of matrix $\mathbf{A}$. $\mathbf{A}\otimes\mathbf{B}$ represents the Kronecker product of matrix $\mathbf{A}$ and matrix $\mathbf{B}$. Finally, $\mathbf{A}\odot\mathbf{B}$ denotes the Hadamard product of matrix $\mathbf{A}$ and matrix $\mathbf{B}$.

II. System Model

We consider a RIS-aided THz communication system in this paper, where the direct path between the base station (BS) and the user equipment (UE) is blocked.[2] The BS employing an N_t-antenna uniform linear array (ULA) serves the single-antenna UE assisted by the RIS composed of an N-element uniform planar array (UPA), as shown in Fig. 1. The RIS is placed in the xy-plane, which has N_1 elements in the horizontal direction and N_2 elements in the vertical direction satisfying $N = N_1 \times N_2$. The bandwidth B is equally divided into M orthogonal subcarriers, where the center frequency can be denoted by f_c. The frequency of the m-th subcarrier for $\forall m = 1, 2, \ldots, M$ is given by

$$f_m = f_c + \frac{B}{M}(m - 1 - \frac{M-1}{2}). \tag{1}$$

Let c denote the speed of light. The antenna spacing d of the RIS and the BS's array is set to half of the carrier wavelength [27], [28], i.e.,

$$d = \frac{c}{2f_c}. \tag{2}$$

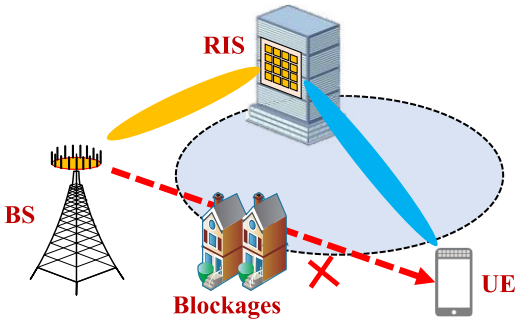

Fig. 1. The RIS-aided THz communication system.

The received signal at the m-th subcarrier y_m is given by

$$y_m = \mathbf{h}_m^T \mathbf{\Theta} \mathbf{G}_m \mathbf{x}_m + n_m, \tag{3}$$

where $\mathbf{x}_m = \mathbf{w} s_m \in \mathbb{C}^{N_t \times 1}$ denotes the transmitted signal at the BS. $s_m \in \mathbb{C}$ represents the transmitted information symbol at the m-th subcarrier satisfying $E[|s_m|^2] = 1$ and $\mathbf{w} \in \mathbb{C}^{N_t \times 1}$ represents the precoding vector. n_m denotes the additive white Gaussian noise (AWGN) with zero mean and variance σ^2. $\mathbf{G}_m \in \mathbb{C}^{N \times N_t}$ is the BS-RIS channel. $\mathbf{h}_m^T = [h_{m,1}, h_{m,2}, \ldots, h_{m,N}] \in \mathbb{C}^{1 \times N}$ represents the channel from the RIS to the UE at the m-th subcarrier. The reflection coefficients of the RIS can be denoted as

$$\mathbf{\Theta} = \mathrm{diag}(\boldsymbol{\theta}) = \mathrm{diag}([e^{j\theta_1}, e^{j\theta_2}, \ldots, e^{j\theta_N}]^T), \tag{4}$$

where the constant reflection amplitude constraint is assumed at the RIS [17], [35].

In this paper, the wideband ray-based channel model is adopted [8]. We define the path delay and the path gain of the BS-RIS channel as $\tau_1 \in \mathbb{R}^+$ and $g_1(f_m, d_1) \in \mathbb{C}$, respectively. The path gain can be expressed as [24], [36], [37], [38]

$$g_1(f_m, d_1) = \frac{c}{4\pi f_m d_1} e^{-\frac{1}{2}\tau_{abs}(f_m) d_1}, \tag{5}$$

where $\tau_{abs}(f_m)$ denotes the molecular absorption factor and d_1 represents the distance between the RIS and BS. The elevation angle and the azimuth angle of the angle-of-arrival (AoA) of the RIS are denoted as ϑ_1^r and ζ_1^r, respectively. The transmit angle of the BS is denoted as ϕ. It is assumed that only the line-of-sight (LoS) path exists by selecting a proper location of RIS deployment.[3] Thus, the BS-RIS channel can be given by

$$\mathbf{G}_m = g_1(f_m, d_1) e^{-j2\pi\tau_1 f_m} \mathbf{a}(f_m, \vartheta_1^r, \zeta_1^r) \mathbf{b}^H(f_m, \phi), \tag{6}$$

where $\mathbf{a}$ denotes the steering vector of the UPA, which can be expressed as

$$\mathbf{a}(f_m, \vartheta, \zeta) = \frac{1}{\sqrt{N_1 N_2}} \left[1, \ldots, e^{j2\pi \frac{f_m}{c}(N_1 - 1) d \sin\vartheta \cos\zeta}\right]^T \otimes \left[1, \ldots, e^{j2\pi \frac{f_m}{c}(N_2 - 1) d \sin\vartheta \sin\zeta}\right]^T, \tag{7}$$

[2]For simplifying the description, we assume that the single UE is served by the RIS without the direct path between the BS and the UE. The results can be extended to the scenario with multiple UEs by deploying multiple RISs [12], [34]. The service of multiple UEs by a single RIS with TD modules is left for future work. The discussions can also be applied to the scenario with the direct path by modifying the equivalent channel model accordingly and utilizing hybrid precoding at the BS [8].

[3]Due to the propagation attenuation and quasi-optical characteristics of THz signals, the LoS path is generally dominated [32], [39].

and $\mathbf{b}$ denotes the steering vector of the ULA, which can be expressed as [8]

$$\mathbf{b}\left(f_m,\phi\right)=\frac{1}{\sqrt{N_{\mathrm{t}}}}\left[1,\ldots,e^{j2\pi\frac{f_m}{c}(N_{\mathrm{t}}-1)d\sin\phi}\right]^T. \quad (8)$$

Similarly, the RIS-UE channel can be expressed as

$$\mathbf{h}_m=g_2(f_m,d_2)e^{-j2\pi\tau_2 f_m}\mathbf{a}\left(f_m,\vartheta_2^t,\zeta_2^t\right), \quad (9)$$

where $\tau_2\in\mathbb{R}^+$ and $g_2(f_m,d_2)\in\mathbb{C}$ denote the path delay and the path gain of the RIS-UE channel, respectively. $g_2(f_m,d_2)$ can be defined as

$$g_2(f_m,d_2)=\frac{c}{4\pi f_m d_2}e^{-\frac{1}{2}\tau_{abs}(f_m)d_2}, \quad (10)$$

where d_2 represents the distance between the RIS and UE. ϑ_2^t and ζ_2^t represent the elevation angle and the azimuth angle of the angle-of-departure (AoD), respectively. The angles satisfy $\vartheta\in\mathcal{U}(0,\pi/2)$, $\zeta\in\mathcal{U}(-\pi,\pi)$, and $\phi\in\mathcal{U}(-\pi/2,\pi/2)$.

Based on the system model, the array gain at the m-th subcarrier is given by

$$\begin{aligned}\eta(f_m)&=\left|\mathbf{h}_m^T\mathbf{\Theta}\mathbf{G}_m\mathbf{w}\right|\\&=\left|g_1(f_m,d_1)g_2(f_m,d_2)e^{-j2\pi(\tau_1+\tau_2)f_m}\right|\\&\quad\cdot\left|\mathbf{a}^T\left(f_m,\vartheta_2^t,\zeta_2^t\right)\mathbf{\Theta}\mathbf{a}(f_m,\vartheta_1^r,\zeta_1^r)\mathbf{b}^H(f_m,\phi)\mathbf{w}\right|,\\&\quad\forall m.\end{aligned} \quad (11)$$

The beam split effect of RIS-aided THz communications will be analyzed in the next section.

III. Beam Split Effect of RIS

In this section, the beam split effect and the resultant array gain loss at the RIS are analyzed. The number of BS antennas is set to $N_t=1$ to simplify the expression. In Section IV, the scenario with a multi-antenna BS will be discussed. To simplify the notations, we define $\alpha_1=\sin\vartheta_1^r\cos\zeta_1^r$, $\beta_1=\sin\vartheta_1^r\sin\zeta_1^r$, $\alpha_2=\sin\vartheta_2^t\cos\zeta_2^t$, $\beta_2=\sin\vartheta_2^t\sin\zeta_2^t$. Besides, we define the relative frequency as $\xi_m=f_m/f_c$. According to (11), the normalized array gain of the RIS at the m-th subcarrier is represented as

$$\begin{aligned}\eta_{\mathrm{RIS}}(f_m)&=\left|\mathbf{a}^T\left(f_m,\vartheta_2^t,\zeta_2^t\right)\mathbf{\Theta}\mathbf{a}(f_m,\vartheta_1^r,\zeta_1^r)\right|\\&=\frac{1}{N_1N_2}\left|\sum_{n_1=0}^{N_1-1}\sum_{n_2=0}^{N_2-1}e^{j\pi\xi_m[n_1(\alpha_1+\alpha_2)+n_2(\beta_1+\beta_2)]}\right.\\&\quad\left.\cdot\,e^{j\theta_k}\right|,\quad k=N_2n_1+n_2+1.\end{aligned} \quad (12)$$

Note that the path gain including the molecular absorption, i.e., $g_1(f_m,d_1)$ or $g_2(f_m,d_2)$, does not affect the normalized array gain. The classical narrowband precoding design of the RIS aims at generating information-carrying beams towards the target physical direction. Thus, we adopt the beamforming vector of the RIS based on the center frequency, which is given by

$$\theta_k=-\pi[n_1(\alpha_1+\alpha_2)+n_2(\beta_1+\beta_2)]. \quad (13)$$

Because of the frequency-independent characteristic of (13), the generated beams cannot be perfectly aligned with the target in the whole bandwidth, which leads to severe array gain loss. To be specific, we have

$$\begin{aligned}&\eta_{\mathrm{RIS}}(f_m)\\&=\frac{1}{N_1N_2}\left|\sum_{n_1=0}^{N_1-1}\sum_{n_2=0}^{N_2-1}e^{j\pi(\xi_m-1)[n_1(\alpha_1+\alpha_2)+n_2(\beta_1+\beta_2)]}\right|\\&\overset{(a)}{=}\left|\Xi_{N_1}((\xi_m-1)(\alpha_1+\alpha_2))\Xi_{N_2}((\xi_m-1)(\beta_1+\beta_2))\right|,\end{aligned} \quad (14)$$

where (a) comes from the equation $\Sigma_{n=0}^{N-1}e^{jn\pi x}=\frac{\sin\frac{N\pi}{2}x}{\sin\frac{\pi}{2}x}e^{-j\frac{(N-1)\pi}{2}x}$ and $\Xi_N(x)=\frac{\sin N\pi x/2}{N\sin\pi x/2}$ is the Dirichlet Sinc Function (DSF).

Then, we provide the normalized array gain at the center frequency f_c and two edge subcarriers f_1 and f_M achieved by the frequency-independent beamforming vector in Fig. 2. The elevation angle and the azimuth angle of the AoA are adopted as $\vartheta_1^r=\pi/4$ and $\zeta_1^r=\pi/2$, respectively. The angles of the AoD are set to $\vartheta_2^t=\pi/4$ and $\zeta_2^t=0$. As shown in Fig. 2 (a), the three beams totally split into distinct directions in the 3-dimensional view. The three views are shown in Fig. 2 (b)-(d), respectively, which also reveal that the generated beams are separated along both elevation angles and azimuth angles. Besides, we choose a specific physical direction as the fixed elevation angle and azimuth angle where the maximum array gain is located. The normalized array gain of different elevation angles with the fixed azimuth angle and that of different azimuth angles with the fixed elevation angle in the 2-dimensional view are shown in the upper and lower figures of Fig. 3, respectively. The generated beam at the center frequency f_c serves as the baseline. The generated beams at edge subcarriers $m=1$ and $m=M$ are provided for comparison. It is observed that the beams at edge subcarriers seriously deviate from the target physical direction.

We further provide the normalized array gain at different subcarriers in Fig. 4. One can observe that the array gain loss increases with the increase of the bandwidth. With the bandwidth of 10 GHz, the classical narrowband precoding, e.g., [9] and [12], suffers 70% gain loss at more than 50%

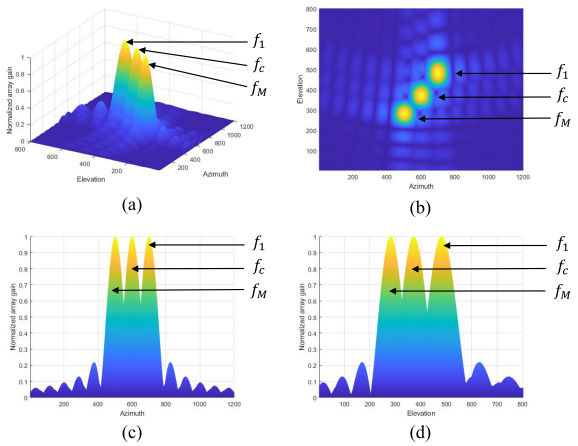

Fig. 2. Beam split at the RIS: (a) 3-dimensional view; (b) Bird-eye's view; (c) Side-view; (d) Front-view.

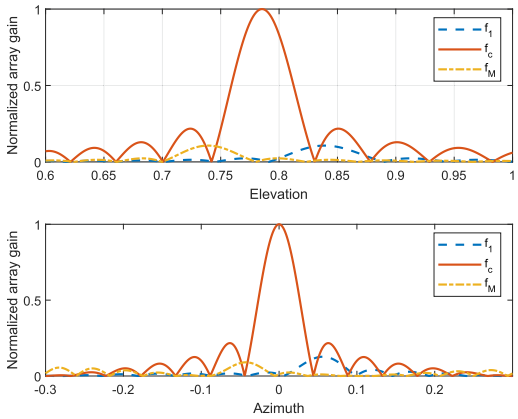

Fig. 3. The normalized array gain versus different angles.

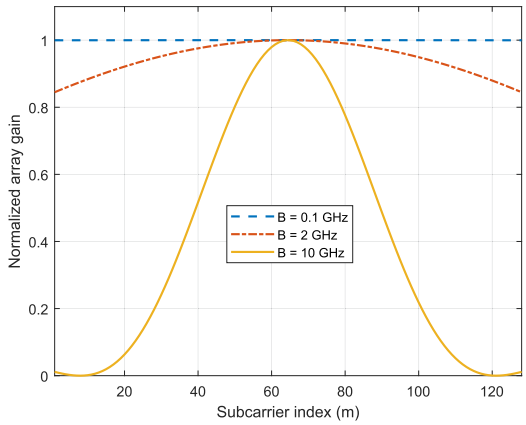

Fig. 4. The normalized array gain versus the subcarrier index.

of the total subcarriers. Thus, the severe gain loss incurred by beam split due to the large bandwidth and the enormous number of RIS elements neutralizes benefits introduced by the exploitation of RIS and the THz spectral resources.

In the next section, the joint phase and delay wideband precoding design will be proposed to deal with the beam split effect.

IV. Proposed SPDP-Based Wideband Precoding Design

In this section, a sub-connected phase-delay-phase architecture (SPDP)-based wideband precoding design is proposed to address the beam split problem in RIS-aided THz communications. First, the SPDP with additional time-delay (TD) modules and low-resolution phase shifters is introduced in Section IV-A. Next, a frequency-dependent wideband precoding design is provided and the normalized array gain is derived to analyze the performance of the proposed SPDP in Section IV-B. Finally, the double beam split effect with massive antennas at the BS is revealed and solved in Section IV-C.

A. Proposed Sub-Connected Phase-Delay-Phase Architecture

In this subsection, based on the existing delay-phase fully-connected architecture with each RIS element equipped with a TD module [29], we propose the SPDP to reduce the

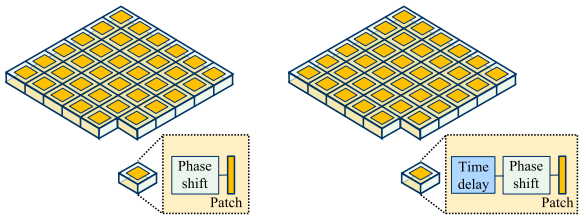

Fig. 5. The RIS architecture: (a) The classical RIS; (b) The delay-phase architecture-based RIS.

hardware cost. Compared with the classical RIS shown in Fig. 5 (a), a TD module is deployed in each element of the delay-phase fully-connected architecture-based RIS to realize frequency-dependent precoding, which is shown in Fig. 5 (b) [18], [29]. The frequency-dependent reflection coefficient of the i-th RIS element is expressed as $e^{j(\theta_i - 2\pi\tau_i f_m)}$ in the delay-phase architecture, where τ_i denotes the time delay. By properly configuring the time delay of each element, the generated beams at different carriers will be aligned with the target. In this way, the beam split effect can be totally eliminated. However, the power consumption and hardware cost of TD modules are generally much higher compared with the counterparts adopting phase shifters only.

Inspired by our prior works on delay-phase precoding [8] in wideband THz communications, a sub-connected architecture for RIS is preferred. Nevertheless, the sub-connected architecture in [8] cannot be directly utilized for RIS. Specifically, the sub-connected BS is separated into several sub-arrays and each sub-array is connected to a TD module. Thus, the elements in a sub-array can provide the desired time delay. However, if the sub-connected delay-phase architecture is directly applied to RIS, the received signals at sub-arrays will first pass through the common TD module and will be mixed together incoherently. The possible resultant destructive interference would lead to severe signal attenuation. Thus, the sub-connected delay-phase architecture with an additional TD module for each sub-array of RIS is infeasible in practice.

To tackle this problem, we adopt additional phase shifters and propose the SPDP-based RIS, as shown in Fig. 6. Specifically, each element of the sub-array is equipped with two-layer phase shifters and is connected to a common TD module based on a circulator. The received signal at each element first passes through the first-layer phase shifter, which aims at creating constructive received signal superposition at the sub-array. Then, the signal is adjusted by the common TD module. Finally, the signal passes through the second-layer phase shifter to accomplish the beamforming of the RIS. In practice, the proposed SPDP-based RIS can also be implemented by exploiting two smaller patches instead of one patch in each antenna based on the planar inverted-F antenna [40]. Besides, the SPDP-based RIS can be implemented as a transmission array, where two-layer phase shifters can be deployed at two sides of the array, respectively [33].

Note that the integrated phase shifters can adopt low-resolution components to further reduce power consumption

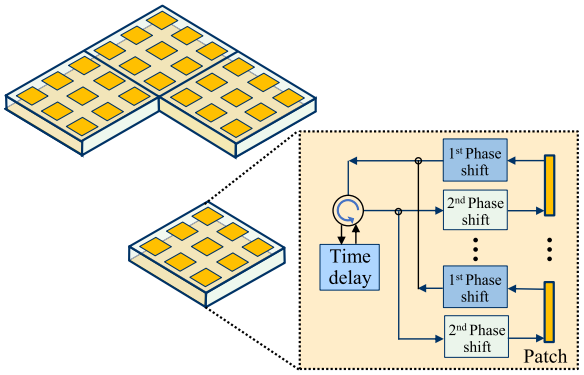

Fig. 6. The proposed SPDP-based RIS, where "1st" represents the first-layer, and "2nd" represents the second-layer.

and hardware cost [41]. For example, the typical power consumption of a TD module is about $P_{\text{TD}} = 100$ mW [8], while that of a phase shifter is $P_{\text{PS}} = 1.5$ mW for adopting 3-bit phase shifting [10]. For the RIS-aided THz communication system, we assume that the RIS is divided into $Q = Q_1 \times Q_2$ sub-arrays, each of which is connected to a TD module. Each sub-array consists of $K = K_1 \times K_2$ elements, where $K_1 = \frac{N_1}{Q_1}$, $K_2 = \frac{N_2}{Q_2}$. Note that K_1 and K_2 can be integers through careful design. For simplifying the expression, let q_1 and q_2 denote the indexes of sub-arrays with $q_1 = 0, 1, \ldots, Q_1 - 1$, and $q_2 = 0, 1, \ldots, Q_2 - 1$. Let k_1 and k_2 denote the indexes of elements in each sub-array with $k_1 = 0, 1, \ldots, K_1 - 1$, and $k_2 = 0, 1, \ldots, K_2 - 1$. The parameters are set to $N_1 = 64$, $N_2 = 64$, $Q_1 = 8$, and $Q_2 = 8$. The total power consumption of the delay-phase architecture is $P_{\text{FC}} = N_1 N_2 (P_{\text{TD}} + P_{\text{PS}}) = 415.7$ W, while that of our proposed SPDP is only $P_{\text{SPDP}} = 2N_1 N_2 P_{\text{PS}} + Q_1 Q_2 P_{\text{TD}} = 18.7$ W, which is much lower than that of the delay-phase architecture. Therefore, our proposed scheme can provide a sub-optimal solution with acceptable power consumption and hardware cost.[4]

Then, we will formulate the signal transmission model based on the proposed SPDP. We reformulate the involved channels as

$$\mathbf{G}_m = \frac{g_1(f_m, d_1)}{\sqrt{N_1 N_2}} e^{-j2\pi\tau_1 f_m} \mathbf{F}\left(f_m, \vartheta_1^r, \zeta_1^r\right), \tag{15}$$

$$\mathbf{H}_m = \frac{g_2(f_m, d_2)}{\sqrt{N_1 N_2}} e^{-j2\pi\tau_2 f_m} \mathbf{F}\left(f_m, \vartheta_2^t, \zeta_2^t\right). \tag{16}$$

$\mathbf{F}$ denotes the steering matrix with the (n_1, n_2)-th element of $\mathbf{F}$ expressed as

$$\mathbf{F}_{(n_1,n_2)}\left(f_m, \vartheta, \zeta\right) = e^{j\pi\xi_m(n_1\alpha + n_2\beta)}, \tag{17}$$

where $\alpha = \sin\vartheta\cos\zeta$, $\beta = \sin\vartheta\sin\zeta$, $n_1 = q_1 K_1 + k_1$, $n_2 = q_2 K_2 + k_2$. We divide the channel model $\mathbf{G}_m$ and $\mathbf{H}_m$ in (15), (16) into partitioned matrices. For example, $\mathbf{G}_m^{(q)}$ corresponds to the q-th sub-array of RIS. Let $t_q \in \mathbb{R}^+$, $\mathbf{\Theta}_1^{(q)}$, and $\mathbf{\Theta}_2^{(q)}$ denote the time delay, the first-layer phase shifting, and the second-layer phase shifting of the q-th sub-array, respectively, where $q = q_1 Q_2 + q_2 + 1$. The time delay vector of the RIS can be expressed as

$$\mathbf{p}_m = e^{-j2\pi f_m \mathbf{t}}, \quad \mathbf{t} = [t_1, t_2, \ldots, t_q, \ldots, t_{Q_1 \times Q_2}]^T. \tag{18}$$

Thus, the signal passing through the first-layer phase shifter of the q-th sub-array of RIS is expressed as

$$y_{1,m}^{(q)} = \text{sum}\left(\mathbf{\Theta}_1^{(q)} \odot \mathbf{G}_m^{(q)} s_m\right). \tag{19}$$

The received signal at the UE, passing through the second-layer phase shifter, can be expressed as

$$y_{2,m}^{(q)} = \text{sum}\left(\mathbf{H}_m^{(q)} \odot (\mathbf{\Theta}_2^{(q)} p_m^{(q)} y_{1,m}^{(q)})\right). \tag{20}$$

According to (19), (20), the array gain of the q-th sub-array of RIS at the m-th subcarrier is expressed as

$$\eta_s(p_m^{(q)}, f_m) = \Big|\text{sum}\Big(\mathbf{H}_m^{(q)} \odot \Big[\mathbf{\Theta}_2^{(q)} p_m^{(q)} \cdot \text{sum}\left(\mathbf{\Theta}_1^{(q)} \odot \mathbf{G}_m^{(q)}\right)\Big]\Big)\Big|, \ \forall m. \tag{21}$$

It can be revealed from (21) that extra time delay and phase shifting are introduced as new design degrees of freedom. As a result, the proposed SPDP is capable of achieving high array gain at different subcarriers, which mitigates the beam split effect.

B. Wideband Precoding Design of SPDP

In this subsection, the array gain of our proposed SPDP-based RIS will be analyzed, and a frequency-dependent wideband precoding design will be proposed to compensate for the gain loss due to beam split. Besides, a low-resolution phase shifters-based practical implementation will be proposed to further reduce power consumption and hardware cost.

Based on (21), the array gain of RIS at the m-th subcarrier can be derived as

$$\eta(\mathbf{p}_m, f_m) = \Big|\sum_{q_1}\sum_{q_2}\Big\{\text{sum}\Big(\mathbf{H}_m^{(q)} \odot \Big[\mathbf{\Theta}_2^{(q)} p_m^{(q)} \cdot \text{sum}\left(\mathbf{\Theta}_1^{(q)} \odot \mathbf{G}_m^{(q)}\right)\Big]\Big)\Big\}\Big|, \quad \forall m. \tag{22}$$

The wideband precoding design based on the SPDP aims at maximizing the array gain of RIS, which can be formulated as

$$\mathcal{P}_1: \max_{\mathbf{\Theta}_1, \mathbf{\Theta}_2, \mathbf{t}} \frac{1}{M}\sum_{m=1}^{M} \eta(\mathbf{p}_m, f_m). \tag{23}$$

We first focus on maximizing the array gain of RIS at the m-th subcarrier $\eta(\mathbf{p}_m, f_m)$. The following lemma provides the solution to the optimization problem $\max \eta(\mathbf{p}_m, f_m)$.

Lemma 1: The wideband precoding design based on the proposed SPDP achieves the optimal performance at the m-th subcarrier, if and only if (24) to (26) are satisfied.

$$t_q = \frac{1}{2f_c}[(q_1 K_1 - (K_1 - 1)/2)(\alpha_1 + \alpha_2) + (q_2 K_2 - (K_2 - 1)/2)(\beta_1 + \beta_2)]. \tag{24}$$

$$\mathbf{\Theta}_1^{(q)}(k_1, k_2) = \mathbf{F}_{(k_1,k_2)}\left(f_c, -\vartheta_1^r, \zeta_1^r\right), \tag{25}$$

$$\mathbf{\Theta}_2^{(q)}(k_1, k_2) = \mathbf{F}_{(k_1,k_2)}\left(f_c, -\vartheta_2^t, \zeta_2^t\right). \tag{26}$$

[4]The performance gap between the optimal scheme and our proposed one will be verified in Section V.

Proof: Since sum $\left(\mathbf{\Theta}_1^{(q)} \odot \mathbf{G}_m^{(q)}\right)$ is a scalar, the optimization problem $\max \eta(\mathbf{p}_m, f_m)$ is equivalent to the joint optimization problems of $\max$ sum $\left(\mathbf{H}_m^{(q)} \odot \mathbf{\Theta}_2^{(q)}\right)$ and $\max$ sum $\left(\mathbf{\Theta}_1^{(q)} \odot \mathbf{G}_m^{(q)}\right)$. The (k_1, k_2)-th element of the q-th partitioned matrices of $\mathbf{G}_m$ can be expressed as

$$\begin{aligned}\mathbf{G}_{m}{}_{(k_1,k_2)}^{(q)} &= \frac{g_1(f_m, d_1)}{\sqrt{N_1 N_2}} e^{-j2\pi\tau_1 f_m} e^{j\pi\xi_m(n_1\alpha_1 + n_2\beta_1)} \\ &= \frac{g_1(f_m, d_1)}{\sqrt{N_1 N_2}} e^{-j2\pi\tau_1 f_m} e^{j\pi\xi_m(q_1 K_1\alpha_1 + q_2 K_2\beta_1)} \\ &\quad \cdot e^{j\pi\xi_m(k_1\alpha_1 + k_2\beta_1)}. \end{aligned} \tag{27}$$

The first-layer phase shifting is determined according to the center frequency, i.e., the solution of $\max$ sum $\left(\mathbf{\Theta}_1^{(q)} \odot \mathbf{G}_m^{(q)}\right)$ is given by

$$\mathbf{\Theta}_1{}_{(k_1,k_2)}^{(q)} = e^{-j\pi(k_1\alpha_1 + k_2\beta_1) - j\phi_1^{(q)}}, \tag{28}$$

where $\phi_1^{(q)}$ is utilized to increase the degrees of freedom. Then, we can ignore the item $e^{-j2\pi\tau_1 f_m}$ whose modulus is 1 and derive that

$$\begin{aligned}&\text{sum}\left(\mathbf{\Theta}_1^{(q)} \odot \mathbf{G}_m^{(q)}\right) \\ &= \frac{g_1(f_m, d_1)}{\sqrt{N_1 N_2}} e^{j\pi\xi_m(q_1 K_1\alpha_1 + q_2 K_2\beta_1)} \\ &\quad \cdot \sum_{k_1}\sum_{k_2} e^{j\pi(\xi_m - 1)(k_1\alpha_1 + k_2\beta_1)} \\ &= \frac{K_1 K_2 g_1(f_m, d_1)}{\sqrt{N_1 N_2}} e^{j\pi\xi_m(q_1 K_1\alpha_1 + q_2 K_2\beta_1)} \\ &\quad \cdot e^{-j\pi(K_1 - 1)(\xi_m - 1)\alpha_1/2} \\ &\quad \cdot \Xi_{K_1}((\xi_m - 1)\alpha_1) e^{-j\pi(K_2 - 1)(\xi_m - 1)\beta_1/2} \\ &\quad \cdot \Xi_{K_2}((\xi_m - 1)\beta_1). \end{aligned} \tag{29}$$

Similarly, we can obtain $\mathbf{\Theta}_2{}_{(k_1,k_2)}^{(q)}$ and sum $\left(\mathbf{H}_m^{(q)} \odot \mathbf{\Theta}_2^{(q)}\right)$ by replacing $(\alpha_1, \beta_1, \phi_1^{(q)})$ with $(\alpha_2, \beta_2, \phi_2^{(q)})$. Specifically, $\mathbf{\Theta}_2{}_{(k_1,k_2)}^{(q)}$ can be given by

$$\mathbf{\Theta}_2{}_{(k_1,k_2)}^{(q)} = e^{-j\pi(k_1\alpha_2 + k_2\beta_2) - j\phi_2^{(q)}}. \tag{30}$$

By substituting the derived formulas into (22), the normalized array gain is obtained, which is given by

$$\begin{aligned}&\eta(\mathbf{p}_m, f_m) \\ &= \frac{K_1^2 K_2^2}{N_1 N_2} |\Xi_{K_1}((\xi_m - 1)\alpha_1)\Xi_{K_1}((\xi_m - 1)\alpha_2) \\ &\quad \cdot \Xi_{K_2}((\xi_m - 1)\beta_1)\Xi_{K_2}((\xi_m - 1)\beta_2)| \left| \sum_{q_1}\sum_{q_2} \left\{ e^{-j2\pi f_m t_q} \right.\right. \\ &\quad \left.\left. \cdot e^{j\pi\xi_m[(q_1 K_1 - (K_1 - 1)/2)(\alpha_1 + \alpha_2) + (q_2 K_2 - (K_2 - 1)/2)(\beta_1 + \beta_2))]} \right\} \right|. \end{aligned} \tag{31}$$

It can be revealed that (31) is related to f_m. Based on the derived array gain, a frequency-dependent wideband precoding design is required. Thus, in order to alleviate the beam split effect over all the available subcarriers, t_q should be derived to maximize (31) by matching the phases. Specifically, t_q should satisfy $e^{-j2\pi f_m t_q} \cdot e^{j\pi\xi_m[(q_1 K_1 - (K_1 - 1)/2)(\alpha_1 + \alpha_2) + (q_2 K_2 - (K_2 - 1)/2)(\beta_1 + \beta_2))]} = 1$, which ensures the constructive interference superposition. Thus, t_q can be given by $t_q = \frac{1}{2f_c}[(q_1 K_1 - (K_1 - 1)/2)(\alpha_1 + \alpha_2) + (q_2 K_2 - (K_2 - 1)/2)(\beta_1 + \beta_2)]$, which is consistent with (24). Besides, $\mathbf{\Theta}_1^{(q)}$ and $\mathbf{\Theta}_2^{(q)}$ can be reformulated as (25) and (26), respectively. ■

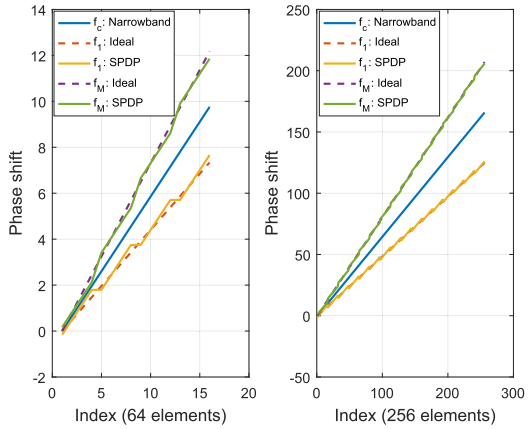

Fig. 7. Phase shift versus the index of RIS elements.

One can observe that the solution, i.e., (24) to (26), to the optimization problem $\max \eta(\mathbf{p}_m, f_m)$ is independent of the subcarrier, which can serve as a closed-form solution to $\mathcal{P}_1$. Then, from **Lemma 1**, the analytical solution of the proposed wideband precoding design based on the SPDP is provided. Note that the value of t_q encourages the alignment between the generated beams and the target physical direction in the whole bandwidth. Besides, $\mathbf{\Theta}_1^{(q)}$ is able to create constructive interference superimposed signals received by different elements at the sub-array. Furthermore, $\mathbf{\Theta}_2^{(q)}$ generates a beam towards the UE at the center frequency. Thus, the normalized array gain achieved by our proposed SPDP-based RIS $\eta(\mathbf{p}_m, f_m)$ can be given by

$$\begin{aligned}&\eta(\mathbf{p}_m, f_m) \\ &= \frac{Q_1 Q_2 K_1^2 K_2^2}{N_1 N_2} |\Xi_{K_1}((\xi_m - 1)\alpha_1)\Xi_{K_1}((\xi_m - 1)\alpha_2) \\ &\quad \cdot \Xi_{K_2}((\xi_m - 1)\beta_1)\Xi_{K_2}((\xi_m - 1)\beta_2)|. \end{aligned} \tag{32}$$

Then, the mechanism of the proposed wideband precoding design is analyzed. According to (12), the optimal beamforming vector of the RIS should be frequency-dependent, which can be expressed as

$$\theta_{\text{opt},k} = -\pi\xi_m[n_1(\alpha_1 + \alpha_2) + n_2(\beta_1 + \beta_2)], \tag{33}$$

We provide the phase shift versus the index of RIS elements in Fig. 7, where the center frequency f_c and two edge subcarriers, f_1 and f_M, respectively, are considered. For simplifying the result, the number of RIS elements and subarrays are set to $N = 1 \times 64$ and $Q = 4$ in the left figure, respectively. The number of RIS elements and subarrays are set to $N = 1 \times 256$ and $Q = 16$ in the right figure, respectively.

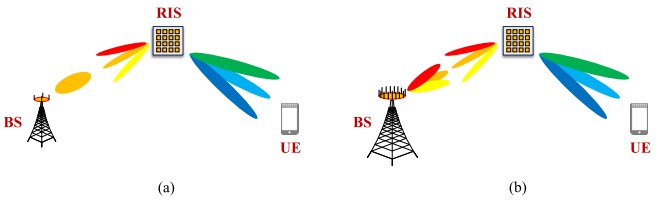

Fig. 8. RIS-aided THz communications: (a) Beam split effect at the RIS; (b) Double beam split effect at the BS and the RIS.

The ideal results come from (33), the result of f_c, i.e., the classical narrowband precoding design, arises from (13), and the results of SPDP come from our proposed wideband precoding design (24) to (26). One can observe that the narrowband precoding design based on (13) cannot generate the desired phase shifts at different subcarriers, which thus results in beam split. By contrast, the proposed SPDP can generate the sub-optimal phase shifts at different subcarriers based on the sub-connected RIS architecture, which alleviates the beam split effect with a small number of TD modules.

Furthermore, we consider a practical implementation based on low-resolution phase shifters. As mentioned in Section IV-A, the low-resolution phase shifters can be adopted in the practical implementation of the proposed SPDP, which further reduces the power consumption and hardware cost. Specifically, after acquiring the continuous phase shifting $\mathbf{\Theta}_i$ of the RIS according to (25), (26), the discrete phase shifting $\mathbf{\Theta}_i^*$ can be obtained by quantization based on the principle of proximity. Let $\mathcal{F}$ denote the set of discrete phase shifts. Then the quantization principle can be expressed as

$$\mathbf{\Theta}_i^*(n_1,n_2) = \arg\min_{\theta\in\mathcal{F}} \left|\theta - \mathbf{\Theta}_i(n_1,n_2)\right|, \quad i=1,2. \tag{34}$$

Note that the obtained discrete phase shifting $\mathbf{\Theta}_1^*$ and $\mathbf{\Theta}_2^*$ can still largely create superimposed signals and generate the directional beam, respectively. Thus, the low-resolution phase shifters-based implementation is capable of providing a better tradeoff with an acceptable performance loss.

C. Solution to Double Beam Split Effect

In this subsection, we extend our discussions from the single antenna to massive antennas at the BS, where the double beam split effect occurs. The decomposability of the array gain is first proved, based on which the joint wideband precoding of the RIS and the BS can be decoupled to simplify the solution.

For a RIS-aided THz communication with massive antennas at the BS, the beam misalignment leads to the double beam split effect, which has not been analytically solved in the literature. Specifically, as illustrated in Fig. 8 (b), the generated beams of the BS with massive antennas at different subcarriers point to different physical directions, which cannot be aligned with the RIS. Besides, the impinging beams and the reflected beams of the RIS cannot be aligned with the BS and the UE in the whole bandwidth, respectively, which also split into separated physical directions. Thus, the RIS-aided THz communication suffers from severe double array gain loss. The following lemma analyzes the array gain $\eta(f_m) = \left|\mathbf{h}_m^T\mathbf{\Theta}\mathbf{G}_m\mathbf{w}\right|$ showing that it can be decomposed into two separated parts.

Lemma 2: $\eta(f_m) = \left|\mathbf{h}_m^T\mathbf{\Theta}\mathbf{G}_m\mathbf{w}\right|$ can be decomposed to $\eta(f_m) = |g_1(f_m,d_1)g_2(f_m,d_2)|\,\eta_{\mathrm{BS}}(f_m)\eta_{\mathrm{RIS}}(f_m)$, where $\eta_{\mathrm{BS}}(f_m)$ and $\eta_{\mathrm{RIS}}(f_m)$ denote the normalized array gain of BS and that of RIS, respectively.

Proof: Based on (11), the array gain can be derived as

$$\begin{aligned}\eta(f_m) &= \left|\mathbf{h}_m^T\mathbf{\Theta}\mathbf{G}_m\mathbf{w}\right| \\ &\overset{(a)}{=} |g_1(f_m,d_1)g_2(f_m,d_2)|\left|\mathbf{a}^T\left(f_m,\vartheta_2^t,\zeta_2^t\right)\mathbf{\Theta}\right. \\ &\quad\left.\cdot\,\mathbf{a}(f_m,\vartheta_1^r,\zeta_1^r)\right|\left|\mathbf{b}^H(f_m,\phi)\mathbf{w}\right|,\end{aligned} \tag{35}$$

wherein (a) comes from the channel characteristic of the LoS path, based on which $\mathbf{b}^H(f_m,\phi)\mathbf{w}$ is a scalar. Note that ϑ_1^r and ζ_1^r denote the elevation angle and the azimuth angle of the AoA, respectively. ϑ_2^t and ζ_2^t denote those of the AoD. Similar to (12), we can define the normalized array gain of the BS as

$$\eta_{\mathrm{BS}}(f_m) = \left|\mathbf{b}^H(f_m,\phi)\mathbf{w}\right|. \tag{36}$$

Thus, $\eta(f_m) = |g_1(f_m,d_1)g_2(f_m,d_2)|\,\eta_{\mathrm{BS}}(f_m)\eta_{\mathrm{RIS}}(f_m)$ can be derived, which completes the proof. ■

From **Lemma 2**, the joint wideband precoding $\max\eta(f_m)$ is equivalent to perform $\max\eta_{\mathrm{BS}}(f_m)$ and $\max\eta_{\mathrm{RIS}}(f_m)$ individually, which aims to separately optimize the wideband precoding of the BS and the wideband precoding of the RIS. That is to say, the double beam split effect can be decomposed such that the joint wideband precoding can be decoupled into two individual frequency-dependent precoding designs to simplify the solution without loss of optimality. In specific, the beam split at the RIS is mitigated by our proposed wideband precoding design based on the SPDP in Section IV-B. The solution to beam split at the BS can be derived similar to the SPDP-based wideband precoding design. In specific, the UPA can be simplified to the ULA with N_t antennas, and the AoA and AoD of the RIS can be simplified to the transmit angle of the BS ϕ. The delay-phase precoding architecture in our previous work on THz massive MIMO precoding [8] is utilized to deal with the beam split effect at the BS. Assuming that the BS is divided into P subarrays, each of which is connected to a TD module. Let $t_p^{\mathrm{BS}} \in \mathbb{R}^+$ and $\mathbf{w}_{u,p}$ denote the time delay and the phase shifting of the p-th sub-array at the BS, respectively. Thus, the frequency-dependent transmit precoding of BS at the m-th subcarrier can be given by

$$\begin{aligned}\mathbf{W}_m &= \mathbf{W}_u\mathbf{p}_m^{\mathrm{BS}} \\ &= \mathrm{blkdiag}([\mathbf{w}_{u,1},\mathbf{w}_{u,2},\ldots,\mathbf{w}_{u,P}]) \\ &\quad\cdot\, e^{-j2\pi f_m\left[t_1^{\mathrm{BS}},t_2^{\mathrm{BS}},\ldots,t_P^{\mathrm{BS}}\right]^T}.\end{aligned} \tag{37}$$

According to the lemma in [8], the time delay vector $\mathbf{p}_m^{\mathrm{BS}}$ and the phase shifting matrix $\mathbf{W}_u$ of the BS should satisfy

$$t_p^{\mathrm{BS}} = \frac{(p-1)(\xi_m-1)N_t\sin\phi}{2f_mP}, \tag{38}$$

$$[\mathbf{w}_{u,1}^T,\mathbf{w}_{u,2}^T,\ldots,\mathbf{w}_{u,P}^T]^T = \mathbf{b}\left(f_c,\phi\right), \tag{39}$$

where $\mathbf{b}$ denotes the steering vector of the ULA in (8). So far we have provided the derivation of the solution to the beam split effect at the BS. Finally, the proposed joint wideband precoding design is summarized in Algorithm 1.

Algorithm 1: Joint Wideband Precoding Design.

Inputs: Transmit angle at the BS ϕ; elevation angle of AoA ϑ_1^r and AOD ϑ_2^t at the RIS; azimuth angle of AOA ζ_1^r and AoD ζ_2^t at the RIS.

Outputs: Transmit precoding of the BS $\mathbf{W}_m$; time delay t_q, first-layer phase shifting $\mathbf{\Theta}_1^{(q)}$, and second-layer phase shifting $\mathbf{\Theta}_2^{(q)}$ of the q-th sub-array of the RIS.

1: Calculate $\alpha_1 = \sin\vartheta_1^r\cos\zeta_1^r$, $\beta_1 = \sin\vartheta_1^r\sin\zeta_1^r$, $\alpha_2 = \sin\vartheta_2^t\cos\zeta_2^t$, $\beta_2 = \sin\vartheta_2^t\sin\zeta_2^t$.
2: Calculate $t_q = \frac{1}{2f_c}[(q_1K_1 - (K_1-1)/2)(\alpha_1+\alpha_2) + (q_2K_2 - (K_2-1)/2)(\beta_1+\beta_2)]$.
3: Calculate $\mathbf{\Theta}_1^{(q)}(k_1,k_2) = \mathbf{F}_{(k_1,k_2)}(f_c, -\vartheta_1^r, \zeta_1^r)$ and $\mathbf{\Theta}_2^{(q)}(k_1,k_2) = \mathbf{F}_{(k_1,k_2)}(f_c, -\vartheta_2^t, \zeta_2^t)$, where $\mathbf{F}_{(n_1,n_2)}(f_m,\vartheta,\zeta) = e^{j\pi\xi_m(n_1\alpha+n_2\beta)}$.
4: **for** $m = 1:M$ **do**
5: Calculate $\mathbf{W}_m = \mathbf{W}_u\mathbf{p}_m^{\mathrm{BS}}$ according to (37)-(39).
6: **end for**

V. Simulation Results

In this section, simulation results are provided to validate the effectiveness of the proposed SPDP by employing the proposed wideband precoding design.

A. Simulation Setup

We consider a RIS-aided THz communication system. The user is located at $(10\text{ m}, 2\text{ m})$. There is a BS located at $(0\text{ m}, 0\text{ m})$ with N_t antennas. Besides, a RIS composed of $N = N_1 \times N_2$ elements is located at $(0\text{ m}, 2\text{ m})$. Note that the square deployment of RIS owns the smaller beam split effect than the rectangular deployment of RIS [28]. Thus, the number of RIS elements is set to $N_1 = 64$ and $N_2 = 64$. The number of subcarriers is set to $M = 128$. The bandwidth is set to $B = 10$ GHz and the center frequency is adopted as $f_c = 100$ GHz. The channel model introduced in Section II is adopted. The molecular absorption loss can be given by 5.157×10^{-4} dB/m, where the ambient temperature, dry air pressure, and water vapor density are set to 15 degrees Celsius, 101325 Pa, and 7.5 g/m^3, respectively [42]. The noise power is given by $\sigma^2 = -120$ dBm. It is assumed that the channel state information (CSI) is perfectly known [9], [10], [11], which can be acquired by the algorithms in [14], [15], and [16].

B. Beamforming Performance

The beamforming performance of our proposed SPDP and the corresponding wideband precoding design is illustrated in this subsection.

According to **Lemma 2**, the double beam split effect of the BS and the RIS can be individually eliminated. For simplifying the result and validating the effect of the proposed SPDP, here we consider a single-antenna BS scenario, where $N_t = 1$. The number of sub-arrays is set to $Q_1 = 8$ and $Q_2 = 8$. The elevation angle and the azimuth angle of the AoA are adopted as $\vartheta_1^r = \pi/4$ and $\zeta_1^r = \pi/2$, respectively. The angles of the AoD are set to $\vartheta_2^t = \pi/4$ and $\zeta_2^t = 0$. The 3-dimensional view and the corresponding three views of the generated beams are shown in Fig. 9, where the generated beams at the center frequency f_c and the edge subcarriers f_1 and f_M are presented. By comparing Fig. 9 with Fig. 2, one can observe that the proposed SPDP with additional TD modules and phase shifters can align the generated beams at different carriers with the target physical direction. The normalized array gain versus different angles at the center frequency f_c and the edge subcarriers f_1 and f_M are shown in Fig. 10. Compared with the misalignment with nearly 100% array gain loss in Fig. 3, it can be observed that the generated beams at the edge subcarriers f_1 and f_M are aligned with the target elevation angle and azimuth angle with only 6% array gain loss. This is because the proposed SPDP is capable of realizing the frequency-dependent precoding, which eliminates the beam split effect.

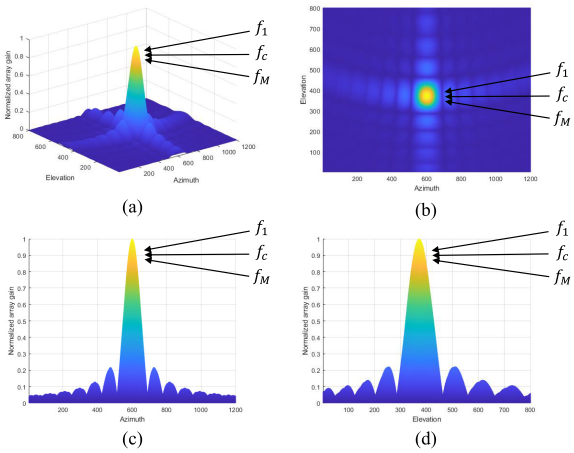

Fig. 9. The generated beams based on the SPDP: (a) 3-dimensional view; (b) Bird-eye's view; (c) Side-view; (d) Front-view.

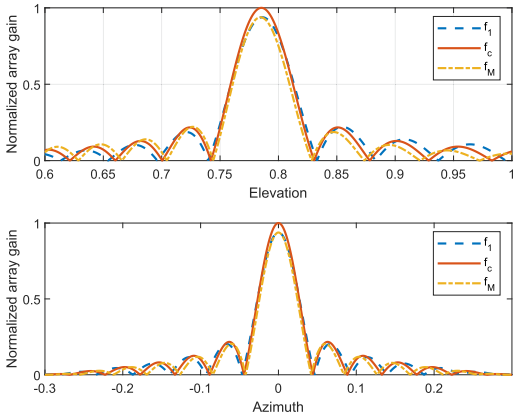

Fig. 10. The normalized array gain versus different angles based on the SPDP.

Furthermore, Fig. 11 shows the normalized array gain at different subcarriers. Compared with Fig. 4, it is revealed that the beam split effect of RIS is significantly alleviated by our proposed SPDP and the corresponding wideband precoding design. Specifically, compared with the narrowband of $B = 0.1$ GHz, the normalized array gain suffers more than 80% loss at subcarrier $m = 20$ with the bandwidth of $B = 10$ GHz. By utilizing the proposed SPDP, the array gain loss can be significantly reduced to about 5%. In other words, the

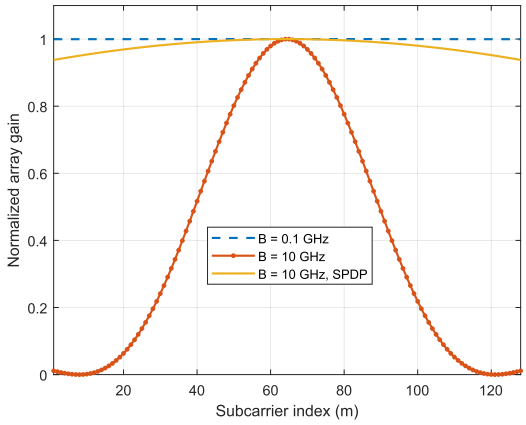

Fig. 11. The normalized array gain versus the subcarrier index based on the SPDP.

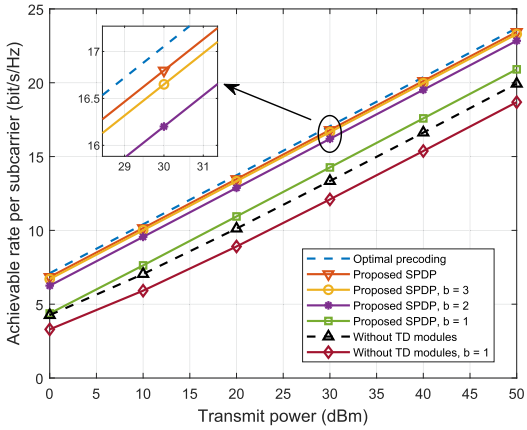

Fig. 12. Average achievable rate per subcarrier versus the transmit power with $N_t = 1,\ Q = 16$.

proposed joint phase and delay wideband precoding design can achieve up to 95% sub-optimal array gain in the whole bandwidth. Thus, the proposed SPDP can serve as an effective wideband precoding solution.

C. Achievable Rate Performance of Single-Antenna BS

In this subsection, the achievable rate performance based on our proposed SPDP is provided in single-antenna BS scenarios, where the beam split of the RIS is considered.

The number of BS antennas is set to $N_t = 1$. In each random experiment, the elevation angles of AoA and AOD of RIS satisfy $\vartheta \sim \mathcal{U}(0, \pi/2)$. The azimuth angles of AOA and AoD of RIS are set to $\zeta \sim \mathcal{U}(-\pi, \pi)$. The average achievable rate per subcarrier versus the transmit power at the BS is provided in Fig. 12. The optimal solution with frequency-dependent precoding design serves as the performance upper bound, where each element is equipped with a TD module. The classical phase-only narrowband beamforming designs with continuous phase shifting and 1-bit phase shifting are adopted as the baseline. The performance of the proposed SPDP is provided with continuous phase shifting and low-resolution phase shifting. The phase shifting resolution is set to $b = 1, 2, 3$ for illustration. The RIS is separated into $Q = 16$ sub-arrays. Note that elements in each sub-array share a common TD

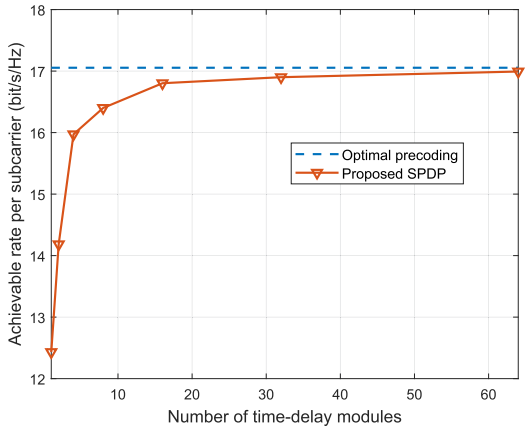

Fig. 13. Average achievable rate per subcarrier versus the number of TD modules.

module. One can observe that the proposed SPDP with 16 TD modules improves the achievable rate by 20% compared with the classical narrowband beamforming design, which can achieve sub-optimal precoding performance. Besides, with only equipping 2-bit phase shifters, the proposed SPDP can closely approach that achieved by the optimal solution, while the former enjoys a lower complexity and hardware cost. The reason is that the proposed SPDP with only low-resolution phase shifters can generate energy-focusing beams towards the target UE through frequency-dependent precoding, which compensates the gain loss due to beam split.

In addition, we provide the average achievable rate per subcarrier versus the number of TD modules, i.e., the number of sub-arrays Q, in Fig. 13. The transmit power is set to 30 dBm and the bandwidth is fixed as $B = 10$ GHz. One can observe that the average achievable rate increases rapidly with the increased number of TD modules. Specifically, the proposed SPDP with merely 4 TD modules can significantly enhance the performance. The proposed SPDP with 16 TD modules is able to achieve a considerable performance of the optimal one, whose hardware cost and power consumption are acceptable. Notice that the performance gap between the proposed SPDP and the optimal precoding decreases slowly as the number of TD modules further increases. In fact, the beam split effect of sub-arrays with fewer elements is less severe than that of the whole RIS. Thus, when the RIS is divided into sub-arrays, a small number of TD modules are sufficient to address the beam split effect. Considering the limited performance growth and extra hardware cost with a large number of TD modules, the segmentation scheme with fewer sub-arrays which provides a better tradeoff is preferred in practice.

D. Achievable Rate Performance With Massive BS Antennas

In this subsection, the achievable rate performance based on our proposed SPDP architecture in multi-antenna BS scenarios with massive BS antennas is provided, where the double beam split effect is considered.

The delay-phase precoding architecture proposed in [8] is utilized to deal with the beam split effect of the BS. The number of BS antennas and TD modules are adopted

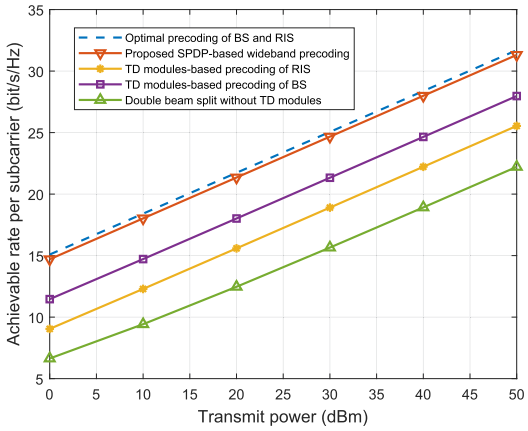

Fig. 14. Average achievable rate per subcarrier versus the transmit power with $N_t = 256,\ Q = 16$.

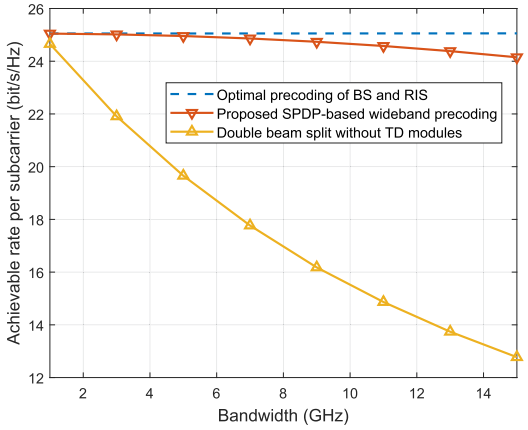

Fig. 15. Average achievable rate per subcarrier versus the bandwidth with $N_t = 256,\ Q = 16$.

as 256 and 16, respectively. In each random experiment, the transmit angle of the BS satisfies $\phi \sim \mathcal{U}(-\pi/2, \pi/2)$. The performance of the proposed SPDP-based joint wideband precoding with continuous phase shifting and $Q = 16$ sub-arrays for the RIS is provided.

The average achievable rate per subcarrier versus the transmit power at the BS is provided in Fig. 14. The optimal frequency-dependent precoding design of the BS and the RIS serves as the performance upper bound. Besides, the frequency-independent narrowband beamforming design without TD modules is employed as the baseline, which results in the double beam split effect. The performance of TD modules-based precoding of the RIS or the BS is also provided for comparison, which corresponds to only tackling the beam split effect at the RIS or the BS based on the sub-connected architecture. It can be observed that compared with the single-antenna BS scenario, the narrowband beamforming design in the multi-antenna BS scenario with massive BS antennas suffers severer achievable rate loss due to double beam split. Besides, the TD modules-based precoding at only one of the BS and the RIS cannot well compensate the performance loss, as they only consider beam split at one of them. In contrast, the proposed SPDP-based joint wideband precoding is capable of achieving sub-optimal achievable rate performance, which mitigates the double beam split effect.

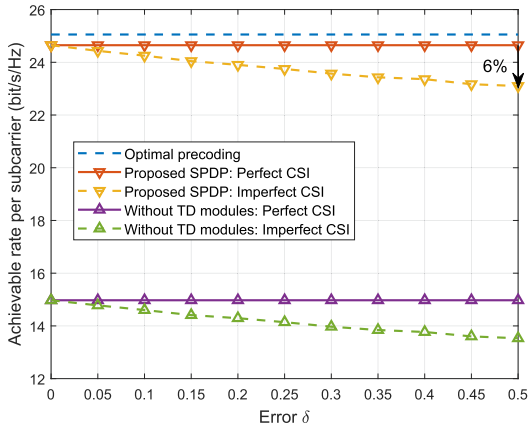

Fig. 16. Average achievable rate per subcarrier versus the error δ.

Besides, the average achievable rate per subcarrier versus the bandwidth in the multi-antenna BS scenario with massive BS antennas is shown in Fig. 15. The transmit power is adopted as 30 dBm. It is revealed that both the proposed SPDP with 16 TD modules and the classical narrowband beamforming can achieve sub-optimal performance when the adopted bandwidth is small. However, the achievable rate of the frequency-independent narrowband beamforming deteriorates rapidly as the bandwidth increases since it cannot address the double beam split effect. By comparison, the proposed SPDP-based joint wideband precoding can compensate the array gain loss caused by the double beam split effect even with large bandwidth, while effectively achieving sub-optimal performance in a wide bandwidth range. Therefore, the proposed SPDP provides a practical solution for RIS-aided THz communications.

Furthermore, we validate the robustness of the proposed wideband precoding design against the impacts of imperfect CSI. Let x and $\hat{x}$ represent the real value and the estimated value of one element in channel matrices $\mathbf{G}_m$ and $\mathbf{h}_m$, which can be modeled as [12]

$$x = \hat{x} + e, \tag{40}$$

where e denotes the independent estimation error following complex Gaussian distribution with zero mean. The normalized mean-square error δ can be expressed as [43]

$$\delta = \frac{E\left[|x - \hat{x}|^2\right]}{E\left[|\hat{x}|^2\right]}. \tag{41}$$

Then, the average achievable rate per subcarrier versus the error δ is shown in Fig. 16. The transmit power is adopted as 30 dBm. One can observe that the performance loss of the proposed SPDP with imperfect CSI increases slowly with the increase of error δ. The reason is that the accuracy of the estimated angles becomes poor with a large error, which results in the beam misalignment. For example, the achievable rate of the SPDP with imperfect CSI suffers 6% loss when $\delta = 0.5$, i.e., the error power is half of the channel gain, compared to that with perfect CSI. Besides, the proposed SPDP always outperforms the frequency-independent beamforming without TD modules at any CSI estimation error, which validates the

effectiveness and robustness of our proposed joint phase and delay wideband precoding to deal with beam split.

VI. Conclusion

The array gain loss of RIS-aided THz communications is severe due to beam split. To tackle this problem, we investigated the joint phase and delay wideband precoding. Specifically, we analyzed the beam split effect and the resultant array gain loss at the RIS. We also proved the decomposability of the double beam split effect at the BS and the RIS. In addition, we proposed a new sub-connected architecture of RIS, based on which a frequency-dependent wideband precoding design with strong robustness to CSI error was proposed to compensate for the gain loss. Our results demonstrated that the proposed SPDP based on ideal phase shifters or low-resolution phase shifters can significantly mitigate the beam split effect, which provided a practical wideband precoding solution for RIS-aided THz communications. Besides, we also revealed that the proposed sub-connected architecture of RIS with a small number of TD modules can provide a more energy-efficient implementation with lower hardware cost and power consumption compared with the optimal phase-delay architecture. The deployment of multiple RISs and the improvement of low-resolution precoding algorithms are left for future works.

References

[1] Z. Chen et al., "Terahertz wireless communications for 2030 and beyond: A cutting-edge frontier," *IEEE Commun. Mag.*, vol. 59, no. 11, pp. 66–72, Nov. 2021.

[2] Z. Chen et al., "A survey on terahertz communications," *China Commun.*, vol. 16, no. 2, pp. 1–35, Feb. 2019.

[3] M. Giordani, M. Polese, M. Mezzavilla, S. Rangan, and M. Zorzi, "Toward 6G networks: Use cases and technologies," *IEEE Commun. Mag.*, vol. 58, no. 3, pp. 55–61, Mar. 2020.

[4] T. S. Rappaport et al., "Wireless communications and applications above 100 GHz: Opportunities and challenges for 6G and beyond," *IEEE Access*, vol. 7, pp. 78729–78757, 2019.

[5] M. D. Renzo et al., "Reconfigurable intelligent surfaces vs. relaying: Differences, similarities, and performance comparison," *IEEE Open J. Commun. Soc.*, vol. 1, pp. 798–807, 2020.

[6] E. Basar, M. Di Renzo, J. De Rosny, M. Debbah, M. Alouini, and R. Zhang, "Wireless communications through reconfigurable intelligent surfaces," *IEEE Access*, vol. 7, pp. 116753–116773, 2019.

[7] S. Hu, F. Rusek, and O. Edfors, "Beyond massive MIMO: The potential of data transmission with large intelligent surfaces," *IEEE Trans. Signal Process.*, vol. 66, no. 10, pp. 2746–2758, May 2018.

[8] L. Dai, J. Tan, Z. Chen, and H. V. Poor, "Delay-phase precoding for wideband THz massive MIMO," *IEEE Trans. Wireless Commun.*, vol. 21, no. 9, pp. 7271–7286, Sep. 2022.

[9] P. Wang, J. Fang, X. Yuan, Z. Chen, and H. Li, "Intelligent reflecting surface-assisted millimeter wave communications: Joint active and passive precoding design," *IEEE Trans. Veh. Technol.*, vol. 69, no. 12, pp. 14960–14973, Oct. 2020.

[10] C. Huang, A. Zappone, G. C. Alexandropoulos, M. Debbah, and C. Yuen, "Reconfigurable intelligent surfaces for energy efficiency in wireless communication," *IEEE Trans. Wireless Commun.*, vol. 18, no. 8, pp. 4157–4170, Aug. 2019.

[11] C. Pan et al., "Multicell MIMO communications relying on intelligent reflecting surfaces," *IEEE Trans. Wireless Commun.*, vol. 19, no. 8, pp. 5218–5233, Aug. 2020.

[12] Z. Zhang and L. Dai, "A joint precoding framework for wideband reconfigurable intelligent surface-aided cell-free network," *IEEE Trans. Signal Process.*, vol. 69, pp. 4085–4101, 2021.

[13] S. Liu, Z. Gao, J. Zhang, M. D. Renzo, and M.-S. Alouini, "Deep denoising neural network assisted compressive channel estimation for mmWave intelligent reflecting surfaces," *IEEE Trans. Veh. Technol.*, vol. 69, no. 8, pp. 9223–9228, Aug. 2020.

[14] Q.-U.-A. Nadeem, H. Alwazani, A. Kammoun, A. Chaaban, M. Debbah, and M.-S. Alouini, "Intelligent reflecting surface-assisted multi-user MISO communication: Channel estimation and beamforming design," *IEEE Open J. Commun. Soc.*, vol. 1, pp. 661–680, 2020.

[15] S. Ma, W. Shen, J. An, and L. Hanzo, "Wideband channel estimation for IRS-aided systems in the face of beam squint," *IEEE Trans. Wireless Commun.*, vol. 20, no. 10, pp. 6240–6253, Oct. 2021.

[16] C. Hu, L. Dai, S. Han, and X. Wang, "Two-timescale channel estimation for reconfigurable intelligent surface aided wireless communications," *IEEE Trans. Commun.*, vol. 69, no. 11, pp. 7736–7747, Nov. 2021.

[17] H. Yang et al., "A 1-bit 10×10 reconfigurable reflectarray antenna: Design, optimization, and experiment," *IEEE Trans. Antennas Propag.*, vol. 64, no. 6, pp. 2246–2254, Jun. 2016.

[18] K. Liu, Z. Zhang, L. Dai, S. Xu, and F. Yang, "Active reconfigurable intelligent surface: Fully-connected or sub-connected?" *IEEE Commun. Lett.*, vol. 26, no. 1, pp. 167–171, Jan. 2022.

[19] H. Li, R. Liu, M. Liy, Q. Liu, and X. Li, "IRS-enhanced wideband MU-MISO-OFDM communication systems," in *Proc. IEEE Wireless Commun. Netw. Conf. (WCNC)*, Seoul, South Korea, May 2020, pp. 1–6.

[20] Z. Wan, Z. Gao, F. Gao, M. Di Renzo, and M.-S. Alouini, "Terahertz massive MIMO with holographic reconfigurable intelligent surfaces," *IEEE Trans. Commun.*, vol. 69, no. 7, pp. 4732–4750, Jul. 2021.

[21] H. Du et al., "Performance and optimization of reconfigurable intelligent surface aided THz communications," *IEEE Trans. Commun.*, vol. 70, no. 5, pp. 3575–3593, May 2022.

[22] P. Wang, J. Fang, W. Zhang, and H. Li, "Fast beam training and alignment for IRS-assisted millimeter wave/terahertz systems," *IEEE Trans. Wireless Commun.*, vol. 21, no. 4, pp. 2710–2724, Apr. 2022.

[23] C. Huang et al., "Multi-hop RIS-empowered terahertz communications: A DRL-based hybrid beamforming design," *IEEE J. Sel. Areas Commun.*, vol. 39, no. 6, pp. 1663–1677, Jun. 2021.

[24] W. Hao et al., "Robust design for intelligent reflecting surface-assisted MIMO-OFDMA terahertz IoT networks," *IEEE Internet Things J.*, vol. 8, no. 16, pp. 13052–13064, Aug. 2021.

[25] A. Liao et al., "Terahertz ultra-massive MIMO-based aeronautical communications in space-air-ground integrated networks," *IEEE J. Sel. Areas Commun.*, vol. 39, no. 6, pp. 1741–1767, Jun. 2021.

[26] Y. Chen, Y. Xiong, D. Chen, T. Jiang, S. X. Ng, and L. Hanzo, "Hybrid precoding for wideband millimeter wave MIMO systems in the face of beam squint," *IEEE Trans. Wireless Commun.*, vol. 20, no. 3, pp. 1847–1860, Mar. 2021.

[27] Y. Chen, D. Chen, and T. Jiang, "Beam-squint mitigating in reconfigurable intelligent surface aided wideband mmWave communications," in *Proc. IEEE Wireless Commun. Netw. Conf. (WCNC)*, Mar. 2021, pp. 1–6.

[28] W. Hao, F. Zhou, M. Zeng, O. A. Dobre, and N. Al-Dhahir, "Ultra wideband THz IRS communications: Applications, challenges, key techniques, and research opportunities," *IEEE Netw.*, vol. 36, no. 6, pp. 214–220, Nov. 2022.

[29] J. An, C. Xu, D. Wing Kwan Ng, C. Yuen, L. Gan, and L. Hanzo, "Reconfigurable intelligent surface-enhanced OFDM communications via delay adjustable metasurface," 2021, *arXiv:2110.09291*.

[30] R. Rotman, M. Tur, and L. Yaron, "True time delay in phased arrays," *Proc. IEEE*, vol. 104, no. 3, pp. 504–518, Mar. 2016.

[31] S.-H. Park, B. Kim, D. Ku Kim, L. Dai, K.-K. Wong, and C.-B. Chae, "Beam squint in ultra-wideband mmWave systems: RF lens array vs. phase-shifter-based array," *IEEE Wireless Commun.*, early access, May 9, 2022, doi: 10.1109/MWC.007.2100530.

[32] M. Di Renzo et al., "Smart radio environments empowered by reconfigurable intelligent surfaces: How it works, state of research, and the road ahead," *IEEE J. Sel. Areas Commun.*, vol. 38, no. 11, pp. 2450–2525, Nov. 2020.

[33] V. Arun and H. Balakrishnan, "RFocus: Beamforming using thousands of passive antennas," in *Proc. 17th USENIX Symp. Netw. Syst. Design Implement. (NSDI)*, Feb. 2020, pp. 1047–1061.

[34] C. You, B. Zheng, W. Mei, and R. Zhang, "How to deploy intelligent reflecting surfaces in wireless network: BS-side, user-side, or both sides?" *J. Commun. Inf. Netw.*, vol. 7, no. 1, pp. 1–10, 2022.

[35] L. Dai et al., "Reconfigurable intelligent surface-based wireless communications: Antenna design, prototyping, and experimental results," *IEEE Access*, vol. 8, pp. 45913–45923, 2020.

[36] C. Lin and G. Y. Li, "Adaptive beamforming with resource allocation for distance-aware multi-user indoor terahertz communications," *IEEE Trans. Commun.*, vol. 63, no. 8, pp. 2985–2995, Aug. 2015.
[37] C. Han and I. F. Akyildiz, "Distance-aware bandwidth-adaptive resource allocation for wireless systems in the terahertz band," *IEEE Trans. Terahertz Sci. Technol.*, vol. 6, no. 4, pp. 541–553, Jul. 2016.
[38] B. Ning, Z. Chen, W. Chen, Y. Du, and J. Fang, "Terahertz multi-user massive MIMO with intelligent reflecting surface: Beam training and hybrid beamforming," *IEEE Trans. Veh. Technol.*, vol. 70, no. 2, pp. 1376–1393, Feb. 2021.
[39] J. Tan and L. Dai, "Wideband beam tracking in THz massive MIMO systems," *IEEE J. Sel. Areas Commun.*, vol. 39, no. 6, pp. 1693–1710, Jun. 2021.
[40] D. M. Nashaat, H. A. Elsadek, and H. Ghali, "Single feed compact quad-band PIFA antenna for wireless communication applications," *IEEE Trans. Antennas Propag.*, vol. 53, no. 8, pp. 2631–2635, Aug. 2005.
[41] C. Huang, G. C. Alexandropoulos, A. Zappone, M. Debbah, and C. Yuen, "Energy efficient multi-user MISO communication using low resolution large intelligent surfaces," in *Proc. IEEE Globecom Workshops (GC Wkshps)*, Abu Dhabi, UAE, Dec. 2018, pp. 1–6.
[42] *Attenuation by Atmospheric Gases*, document ITU-R Rec. P.676-10, Int. Telecommun. Union, Geneva, Switzerland, 2013.
[43] H. Guo, Y.-C. Liang, J. Chen, and E. G. Larsson, "Weighted sum-rate maximization for reconfigurable intelligent surface aided wireless networks," *IEEE Trans. Wireless Commun.*, vol. 19, no. 5, pp. 3064–3076, May 2020.

Ruochen Su (Graduate Student Member, IEEE) received the B.S. degree from the Department of Electronic Engineering, Tsinghua University, Beijing, China, in 2018, where he is currently pursuing the Ph.D. degree. His research interests include reconfigurable intelligent surface (RIS), massive MIMO, and terahertz communications.

Linglong Dai (Fellow, IEEE) received the B.S. degree from Zhejiang University, Hangzhou, China, in 2003, the M.S. degree from the China Academy of Telecommunications Technology, Beijing, China, in 2006, and the Ph.D. degree from Tsinghua University, Beijing, in 2011. From 2011 to 2013, he was a Post-Doctoral Research Fellow with the Department of Electronic Engineering, Tsinghua University, where he was an Assistant Professor from 2013 to 2016, an Associate Professor from 2016 to 2022, and has been a Professor since 2022. His current research interests include massive MIMO, reconfigurable intelligent surface (RIS), millimeter-wave and terahertz communications, machine learning for wireless communications, and electromagnetic information theory.

He has authored or coauthored over 80 IEEE journal articles and over 50 IEEE conference papers. He holds 19 granted patents. He has coauthored the book titled *MmWave Massive MIMO: A Paradigm for 5G* (Academic Press, 2016). He has received five IEEE Best Paper Awards from the IEEE ICC 2013, the IEEE ICC 2014, the IEEE ICC 2017, the IEEE VTC 2017-Fall, and the IEEE ICC 2018. He has also received the Tsinghua University Outstanding Ph.D. Graduate Award in 2011, the Beijing Excellent Doctoral Dissertation Award in 2012, the China National Excellent Doctoral Dissertation Nomination Award in 2013, the URSI Young Scientist Award in 2014, the IEEE Transactions on Broadcasting Best Paper Award in 2015, the Electronics Letters Best Paper Award in 2016, the National Natural Science Foundation of China for Outstanding Young Scholars in 2017, the IEEE ComSoc Asia-Pacific Outstanding Young Researcher Award in 2017, the IEEE ComSoc Asia-Pacific Outstanding Paper Award in 2018, the China Communications Best Paper Award in 2019, IEEE ACCESS Best Multimedia Award in 2020, the IEEE Communications Society Leonard G. Abraham Prize in 2020, the IEEE ComSoc Stephen O. Rice Prize in 2022, and the IEEE ICC Outstanding Demo Award in 2022. He was listed as a Highly Cited Researcher by Clarivate Analytics from 2020 to 2022. Particularly, he is dedicated to reproducible research and has made a large amount of simulation code publicly available.

Derrick Wing Kwan Ng (Fellow, IEEE) received the bachelor's degree with first-class honors and the Master of Philosophy (M.Phil.) degree in electronics engineering from the Hong Kong University of Science and Technology (HKUST), in 2006 and 2008, respectively, and the Ph.D. degree from The University of British Columbia (UBC) in November 2012. He was a Senior Post-Doctoral Fellow with the Institute for Digital Communications, Friedrich-Alexander-University Erlangen–Nürnberg (FAU), Germany. He is currently a Scientia Associate Professor with the University of New South Wales, Sydney, Australia. His research interests include global optimization, physical layer security, IRS-assisted communication, UAV-assisted communication, wireless information and power transfer, and green (energy-efficient) wireless communications.

He received the Australian Research Council (ARC) Discovery Early Career Researcher Award 2017, the IEEE TCGCC Best Journal Paper Award 2018, the IEEE Communications Society Stephen O. Rice Prize 2022, the Best Paper Awards from the WCSP 2020 and 2021, INISCOM 2018, the IEEE International Conference on Communications (ICC) 2018 and 2021, the IEEE International Conference on Computing, Networking and Communications (ICNC) 2016, the IEEE Wireless Communications and Networking Conference (WCNC) 2012, the IEEE Global Telecommunication Conference (Globecom) 2011 and 2021, and the IEEE Third International Conference on Communications and Networking in China 2008. He has been listed as a Highly Cited Researcher by Clarivate Analytics (Web of Science) since 2018. He was an Editorial Assistant to the Editor-in-Chief of the IEEE TRANSACTIONS ON COMMUNICATIONS from January 2012 to December 2019. He is currently an Editor of the IEEE TRANSACTIONS ON COMMUNICATIONS and the IEEE TRANSACTIONS ON WIRELESS COMMUNICATIONS, and an Associate Editor-in-Chief of the IEEE OPEN JOURNAL OF THE COMMUNICATIONS SOCIETY.